DYNAMIC INSTABILITIES OF CIRCULATION CONTROLLED AEROFOILS

Ian Krukow, Nora Neuert and Dieter Dinkler

TU Braunschweig, SFB 880/Institut für Statik
Beethovenstr. 51, 38106 Braunschweig, Germany
statik@tu-bs.de

Keywords: aeroelasticity, circulation control, reduced-order model, modal reduction, flutter

Abstract: The continuously rising volume of air traffic demands for a correspondingly rising capacity of airports. One possible scenario is the extended use of small, existing airports for point-to-point connections. However, in order to use the shorter runways, the high-lift systems have to be improved significantly. This can be achieved by active circulation control making use of the Coandă effect. Though subject to research for several decades, there are still a number of issues to consider in order to make it work for a commercial aircraft. Investigating the aeroelastic behaviour is essential for stability issues. It turns out that the application of active circulation control leads to two additional flutter phenomena, which do not occur with conventional aircraft. Both of them are single degree of freedom flutter – related to heave and pitch motion, respectively – occurring at low velocities as in landing approach.

1 INTRODUCTION

Worldwide air traffic is increasing, and this trend is expected to continue for the next decades. At the same time, the capacity of airports currently in use is limited, and it is difficult to enlarge existing airports or build new ones in highly populated areas. Therefore, it would be desirable to employ smaller airports, which do exist already. However, for shorter runways the efficiency of the high-lift systems has to be increased significantly.

A promising technology is the active circulation control making use of the Coandă effect. Though first described by Thomas Young in 1800 [1] and subject to research in the field of aerodynamics for several decades [2–5], there are atill a number of issues to tackle in order to get it to the maturity needed for commercial aircraft.

One of these issues is the aeroelastic behaviour, which is very little known. The has been some research at the David W. Taylor Naval Ship Research and Development Center with a quasi-elliptical aerofoil. Static aeroelasticity has been studied [6, 7], and an investigation of the flutter behaviour [8] shows an additional flutter phenomenon they termed “circulation control flutter” according to its origin. The phenomenon is single of freedom bending flutter, which does not depend on the approach velocity. These results indicate that the aeroelastic behaviour of a circulation control wing may differ significantly from the behaviour of a conventional wing.

The results presented in this paper were generated as part of the corporate research project Son-

derforschungsbereich 880 [9]. In this project, a Coandă flap is used, i.e. a combination of active circulation control and a conventional flap. This approach allows for flap deflection angles up to 80° without flow separation, resulting in possible lift coefficients greater than 5 [5].

Well-known flutter phenomena like bending-torsion flutter have to be considered like with any conventional wing, but are not described in this paper, which focusses only on the additional phenomena due to the active circulation control. Besides the bending flutter mentioned above, it turns out that there is also a destabilising effect on the pitching motion. Though two separate phenomena, both of them describe single degree of freedom flutter, which may occur at very low velocities as in landing approach.

The additional flutter phenomena are investigated using a two-dimensional aerofoil model. It is commonly known that the active circulation control shifts the stall angle to lower angles of attack. As this behaviour is undesirable, a droop nose is applied, which can prevent the early stall [10]. Following a short introduction of the Coandă flap in Section 2, the aerofoil model is presented in Section 3. The resulting flutter phenomena are described in Section 4.

2 COANDĂ FLAP

A thin jet is much more likely to follow a curved surface than a surrounding free stream flow. This phenomenon is called “Coandă effect”. A conventional trailing-edge flap can be deflected by about 30° before the surrounding flow separates. If a thin jet of air is blown over the upper surface of the flap, the Coandă effect prevents separation, and the flap may be deflected much further. The outblowing is controlled by the dimensionless momentum coefficient

$$c_\mu = \frac{v_{jet}\,\dot{m}_{jet}}{q_\infty A_{ref}}\,, \tag{1}$$

where v_{jet} is the velocity of the jet in the Coandă slot, $\dot{m}_{jet}$ the mass flow in the Coandă slot, q_∞ the dynamic pressure and A_{ref} the reference wing area.

Figure 1 compares the resulting flow field without blowing, $c_\mu = 0$, and with enough blowing to make the flow stay completely attached to flap, $c_\mu = 0.04$, at an angle of attack of $\alpha = 5°$. The aerofoil under investigation is the DLR F15 [11] in the anticipated landing configuration with a flap deflection of $\delta_{fl} = 65°$ and an approach velocity of $u_\infty = 51$ m/s.

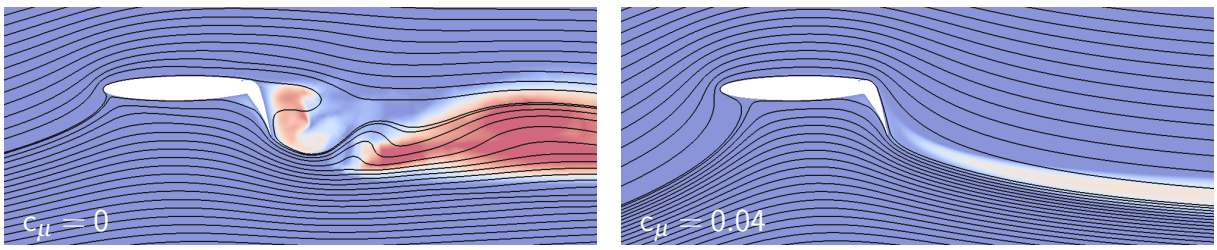

Figure 1: Flow around DLR F15 profile without and with circulation control, $\delta_{fl} = 65°$, $\alpha = 5°$, $u_\infty = 51$ m/s

3 AEROELASTIC AEROFOIL MODEL

In order to investigate the physical phenomena, a two-dimensional aerofoil model is considered as shown in Figure 2. The aerofoil has two degrees of freedom h and α for heave and pitch

motion, respectively, and is held by the corresponding springs. The reference point for all numerical models is the quarter chord, while the center of mass S it at 40 % of the chord length l yielding an eccentricity of $e = 0.15l$. All other parameters are roughly derived from the three-dimensional wing model in [12].

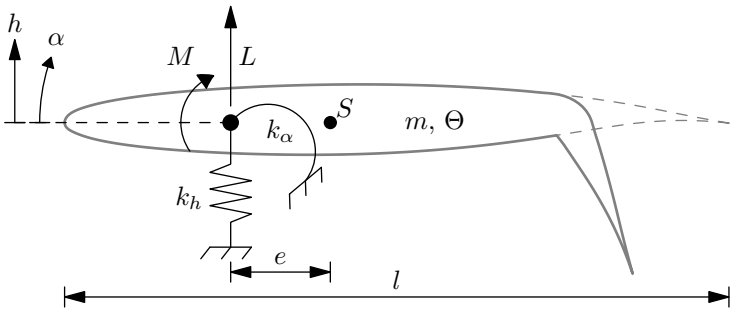

$$l = 3.428 \text{ m}$$
$$k_h = 8.75 \cdot 10^5 \text{ N/m}$$
$$k_\alpha = 1.11 \cdot 10^7 \text{ Nm}$$
$$m = 325 \text{ kg/m}$$
$$\Theta = 313 \text{ kgm}$$

Figure 2: Aeroelastic model of the aerofoil

The aerodynamic loads on the aerofoil are the lift force L and the pitching moment M expressed by their dimensionless coefficients

$$c_L = \frac{L}{q_\infty l}, \quad c_M = \frac{M}{q_\infty l^2}, \tag{2}$$

where q_∞ is the dynamic pressure. Thus, the motion may be described by

$$\begin{bmatrix} m & -e\,m \\ -e\,m & e^2 m + \Theta \end{bmatrix} \begin{bmatrix} \ddot{h} \\ \ddot{\alpha} \end{bmatrix} + \begin{bmatrix} k_h & -e\,k_h \\ -e\,k_h & e^2 k_h + k_\alpha \end{bmatrix} \begin{bmatrix} h \\ \alpha \end{bmatrix} = q_\infty \begin{bmatrix} l\,c_L \\ l^2 c_M \end{bmatrix}. \tag{3}$$

The aerodynamic coefficients are dependent on the profile motion and are described by their derivatives as

$$c_L = c_{L0} + c_{L\alpha}\,\alpha + \frac{1}{u_\infty}\left(c_{L\dot{h}}\,\dot{h} + c_{L\dot{\alpha}}\,l\,\dot{\alpha}\right), \tag{4}$$

$$c_M = c_{M0} + c_{M\alpha}\,\alpha + \frac{1}{u_\infty}\left(c_{M\dot{h}}\,\dot{h} + c_{M\dot{\alpha}}\,l\,\dot{\alpha}\right). \tag{5}$$

The aerodynamic mass terms are ignored. In order to determine the derivatives, numerical flow simulations are performed with the TAU code of the DLR [13]. The results are approximated by polynomial smoothing functions. All following approximations are only valid for a flap deflection of $\delta_{fl} = 65^\circ$ and super circulation, i.e. enough blowing that the flow stays completely attached to the flap. For the given profile, this is achieved by momentum coefficients $c_\mu \geq 0.033$.

3.1 Clean nose

For a clean nose, steady-state simulations provide the coefficients given in Figure 3 along with their smoothing functions

$$\begin{aligned} c_L = {} & 2.95 + 47.5\,c_\mu - 162\,c_\mu^2 + (0.437 + 53.4\,c_\mu - 368\,c_\mu^2)\,\alpha \\ & - (0.456 - 20.8\,c_\mu + 360\,c_\mu^2)\,10^2\,\alpha^2 - (1.34 - 64.4\,c_\mu + 831\,c_\mu^2)\,10^3\,\alpha^3 \\ & - (1.33 - 59.6\,c_\mu + 687\,c_\mu^2)\,10^4\,\alpha^4 - (0.425 - 18.3\,c_\mu + 198\,c_\mu^2)\,10^5\,\alpha^5\,, \end{aligned} \tag{6}$$

$$\begin{aligned} c_M = {} & -0.490 - 9.61\,c_\mu + 28.2\,c_\mu^2 + (1.13 - 7.82\,c_\mu + 90.8\,c_\mu^2)\,\alpha \\ & + (9.33 - 435\,c_\mu + 7.76\cdot 10^3\,c_\mu^2)\,\alpha^2 + (0.275 - 13.3\,c_\mu + 171\,c_\mu^2)\,10^3\,\alpha^3 \\ & + (0.276 - 12.3\,c_\mu + 140\,c_\mu^2)\,10^4\,\alpha^4 + (0.896 - 38.4\,c_\mu + 410\,c_\mu^2)\,10^4\,\alpha^5\,. \end{aligned} \tag{7}$$

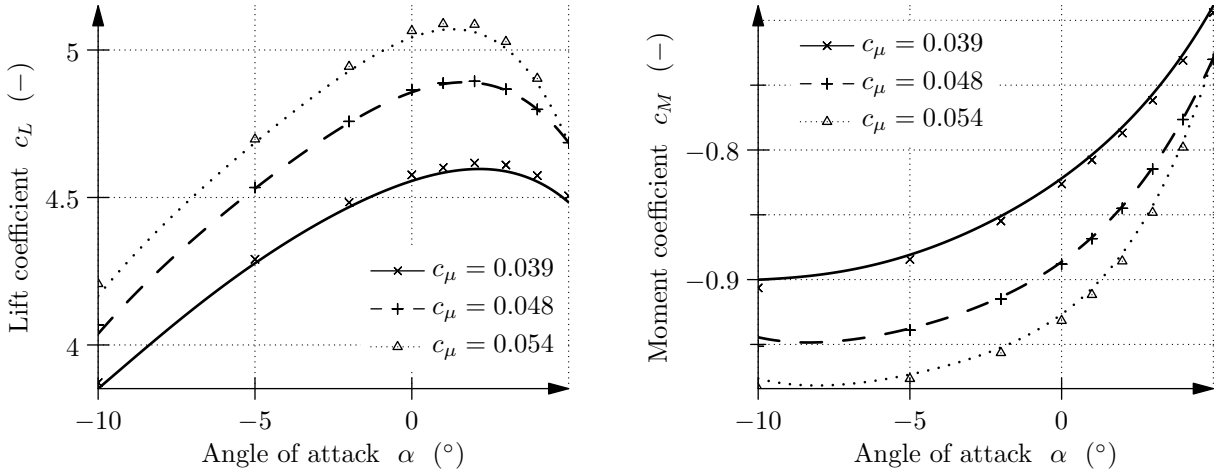

Figure 3: Steady-state coefficients with clean nose

Besides the high lift coefficients of up to 5, the gradual decrease of lift after its maximum is significant. In this regime, the flow is still completely attached, yet special characteristics of the interaction between the Coandă jet and the boundary layer make the circulation control less effective. Therefore, the lift is reduced significantly before stall occurs. This phenomenon has been described as "c_μ-α-stall" in [7].

The steady-state simulations directly yield the derivatives

$$c_{L0} = c_L(\alpha)\,, \qquad c_{M0} = c_M(\alpha)\,, \tag{8}$$

$$c_{L\alpha} = \frac{\partial c_L}{\partial \alpha}(\alpha)\,, \qquad c_{M\alpha} = \frac{\partial c_M}{\partial \alpha}(\alpha)\,. \tag{9}$$

A vertical speed $\dot{h}$ has the same effect as a change in the angle of attack,

$$\dot{h} = -u_\infty\,\alpha_{\dot{h}}\,. \tag{10}$$

Since the free stream velocity has been separated in Eqs. (4) and (5) for non-dimensionality,

$$c_{L\dot{h}} = -c_{L\alpha}\,, \qquad c_{M\dot{h}} = -c_{M\alpha}\,. \tag{11}$$

For the $\dot{\alpha}$-derivatives additional simulations of pitching oscillations are necessary. They are performed with a reduced frequency of $k = 0.36$, which is near the first torsional frequency of the underlying reference wing model. Figure 4 shows the results along with the smoothing functions

$$\begin{aligned} c_{L\dot{\alpha}} &= 3.99 - 142\,c_\mu + 551\,c_\mu^2 + (0.472 - 22.2\,c_\mu + 266\,c_\mu^2)\,10^3\,\alpha \\ &\quad + (1.05 - 54.4\,c_\mu - 750\,c_\mu^2)\,10^4\,\alpha^2 + (1.09 - 57.1\,c_\mu + 796\,c_\mu^2)\,10^5\,\alpha^3 \\ &\quad + (0.382 - 19.7\,c_\mu + 267\,c_\mu^2)\,10^6\,\alpha^4\,, \end{aligned} \tag{12}$$

$$\begin{aligned} c_{M\dot{\alpha}} &= -4.61 + 189\,c_\mu - 1.78\cdot 10^3\,c_\mu^2 - (1.74 - 78.2\,c_\mu + 931\,c_\mu^2)\,10^2\,\alpha \\ &\quad - (0.500 - 24.1\,c_\mu + 302\,c_\mu^2)\,10^4\,\alpha^2 - (0.623 - 30.0\,c_\mu + 368\,c_\mu^2)\,10^5\,\alpha^3 \\ &\quad - (0.233 - 11.1\,c_\mu + 133\,c_\mu^2)\,10^6\,\alpha^4\,. \end{aligned} \tag{13}$$

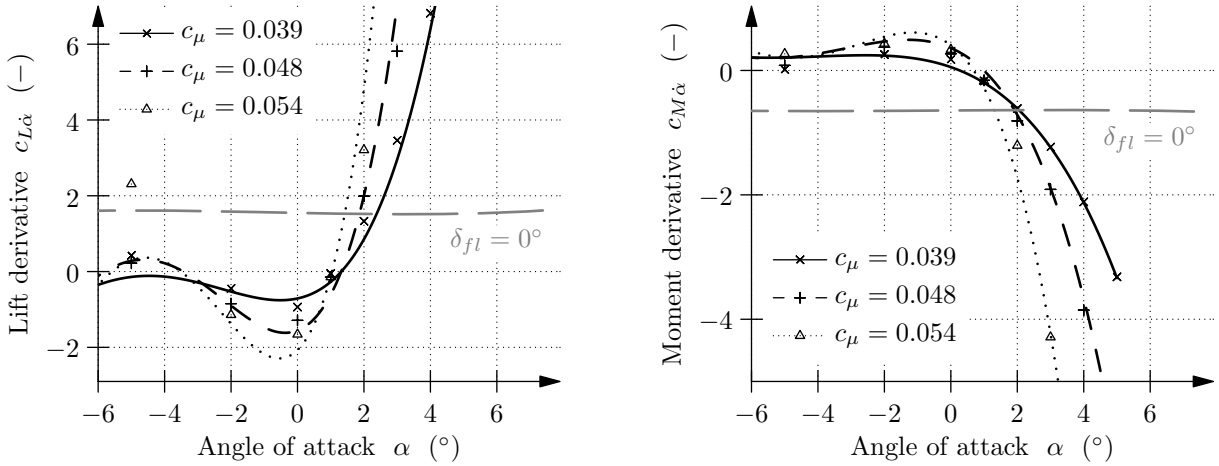

Figure 4: $\dot{\alpha}$-derivatives with clean nose, $k = 0.36$

For comparison, the values without flap deflection are given too. They are almost constant in the given range of angles of attack. Near the stall angle of about 15°, they also show a sudden rise as with $\delta_{fl} = 65°$, but without the characteristic dip before, which even results in a change of sign of both lift and moment derivative.

3.2 Droop nose

Figure 3 shows an angle of attack at maximum lift of about 2° with active circulation control. Considering flight dynamics, this leads to negative angles of attack of about −8° in landing approach [14], which is unacceptable. A promising remedy is found in the application of a droop nose [10], which is sketched in Figure 5.

Figure 6 compares the pressure distributions with clean and droop nose. Both of them show the suction area on the flap due to the active circulation control. With a clean nose, there is a suction peak at the nose, which is responsible for the low stall angles. It is significantly reduced by the droop nose, thus preventing the early stall.

For the time being, the droop nose is only considered in the aerodynamic submodel. The influence on the structural behaviour is assumed to be negligible. However, this assumption has to be validated when further knowledge is gained concerning its structural implementation.

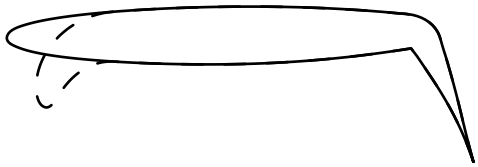

Figure 5: Droop nose

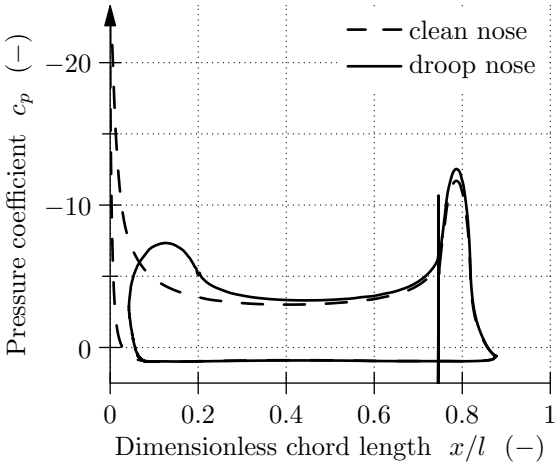

Figure 6: Pressure distribution for $c_\mu = 0.04$, $\alpha = 0°$

Figure 7 shows the changes in the steady-state coefficients resulting from the droop nose. A preliminary, rather rough approximation of the coefficients for the droop nose is obtained by

$$c_{L,droop} = (173 + 203\,\alpha - e^{14.5\,\alpha})\,(0.0191 + 0.192\,c_\mu)\,, \tag{14}$$

$$c_{M,droop} = (-54.8 - 4.06\,\alpha + e^{11.1\,\alpha})\,(0.0112 + 0.151\,c_\mu)\,. \tag{15}$$

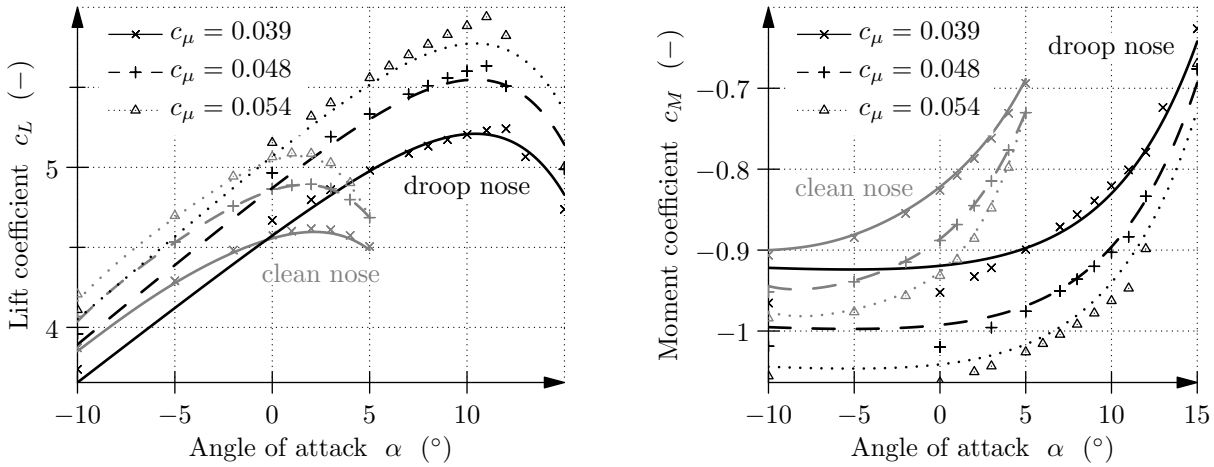

Figure 7: Steady-state coefficients with droop nose

The results show that the stall angle may be shifted by 10° by the droop nose. The lift coefficients are increased accordingly, so that values up to 6 are possible. The moment curves are shifted to higher angles of attack too. Besides, the nose-heavy moment is increased by the droop nose due to the reduction of the suction peak at the nose shown in Figure 6.

For the $\dot{\alpha}$-derivatives from pitching oscillations, there are only results for the optimal momentum coefficient of $c_\mu = 0.033$ available by now. Figure 8 shows the comparison of clean nose and droop nose results. The derivatives with droop nose are approximated roughly by

$$c_{L\dot{\alpha},droop} = -0.857 - 9.65\,\alpha + 90.0\,\alpha^2 + 427\,\alpha^3 - 1240\,\alpha^4\,, \tag{16}$$

$$c_{M\dot{\alpha},droop} = 0.129 - 0.939\,\alpha - 11.4\,\alpha^2\,. \tag{17}$$

Besides the shift of the stall angle, it turns out that the dip resulting in a change of sign is increased significantly by the droop nose.

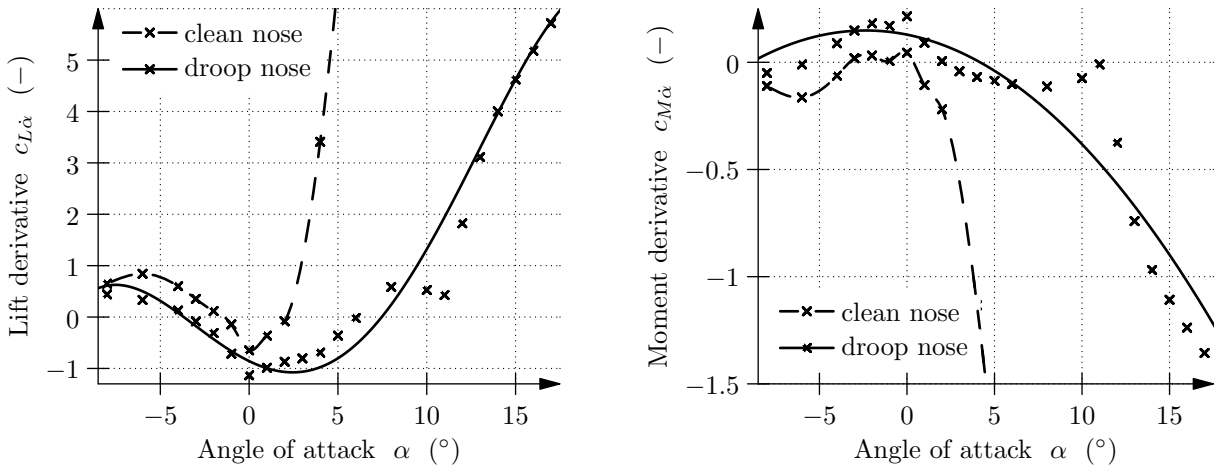

Figure 8: $\dot{\alpha}$-derivatives with droop nose for optimal momentum coefficient $c_\mu = 0.033$, $k = 0.36$

4 FLUTTER

4.1 Bending flutter

Considering a heave oscillation of the aerofoil, the critical derivative is $c_{L\dot{h}}$, which describes the damping term related to the heave motion and the conjugate lift force. A negative value of $c_{L\dot{h}}$ means an additional lift force contrary to the profile motion, as sketched in Figure 9, damping the oscillation. When $c_{L\dot{h}}$ becomes positive, the additional lift force changes its sign too, so that it amplifies the oscillation.

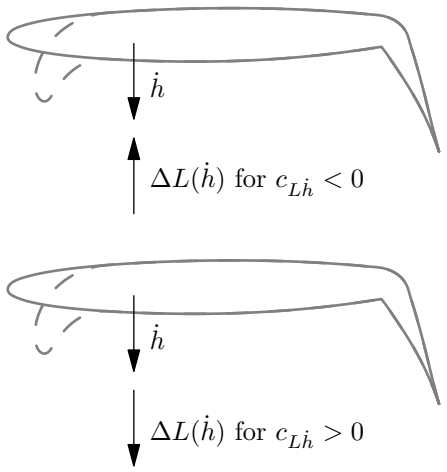

Figure 9: Schematic diagram of bending flutter

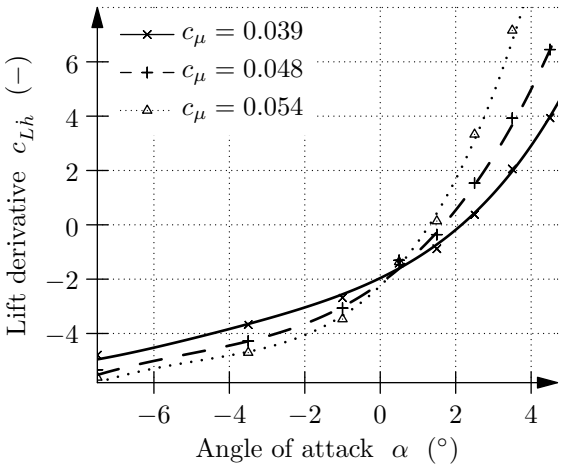

Figure 10: Critical derivative $c_{L\dot{h}}$ with clean nose

Figure 10 shows $c_{L\dot{h}}$ with a clean nose according to Eq. (11) as a function of the angle of attack α for different momentum coefficients c_μ. The zero crossing around $\alpha = 2°$ relates to the maximum of the lift curves in Figure 3. At higher angles of attack, the aerofoil suffers from c_μ-α-stall. Therefore, the lift derivative $c_{L\dot{h}}$ becomes positive resulting in bending flutter as described in [8].

The principle is the same when a droop nose is applied, except that the angle of maximum lift is shifted by about 10°, and therefore the zero crossing, denoting the stability boundary, is shifted likewise, cf. Figure 13.

It should be noticed that this kind of flutter differs significantly from classical bending-torsion-flutter, which starts at a certain velocity due to the interaction of two natural modes, which increases with the velocity. In contrast, bending flutter takes only one natural mode and is independent of the velocity. Thus, it may occur at very low speed as in landing approach, where the circulation control is designed to be active.

4.2 Torsion flutter

For a pitch oscillation, the relevant derivatives are $c_{L\dot{\alpha}}$ and $c_{M\dot{\alpha}}$, which are given in Figure 4 for a clean nose and in Figure 8 for a droop nose. Again, a change of sign in the dynamic derivatives occurs due to the Coandă jet, which is not known from conventional aerofoils. Thus, the pitching oscillation becomes excited for a certain parameter range resulting in torsion flutter.

The pressure distribution in Figure 6 shows two suction areas. At the nose, a pitching oscillation always leads to an additional force contrary to the profile motion, damping the oscillation. At the Coandă slot, however, the additional force may be damping or exciting as sketched in Figure 11, in the latter case leading to torsion flutter.

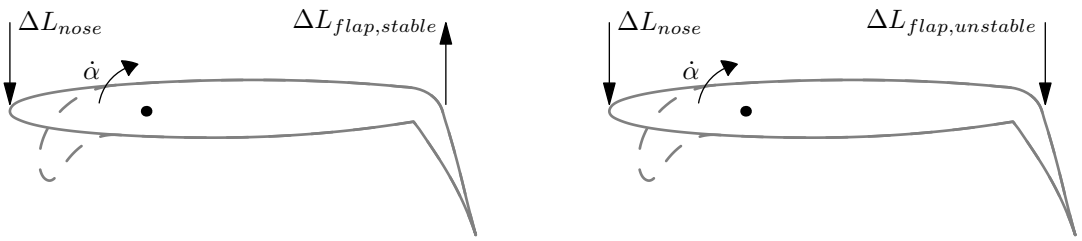

Figure 11: Schematic diagram of torsion flutter

Figure 12 shows the stability boundaries for the two-degree-of-freedom model with a clean nose according to Figure 2 in landing configuration, $\delta_{fl} = 65°$, depending on the momentum coefficient c_μ and the angle of attack α. While bending flutter occurs after the maximum of the lift curve, torsion flutter arises at lower angles of attack, which are more likely to be inside the operation range.

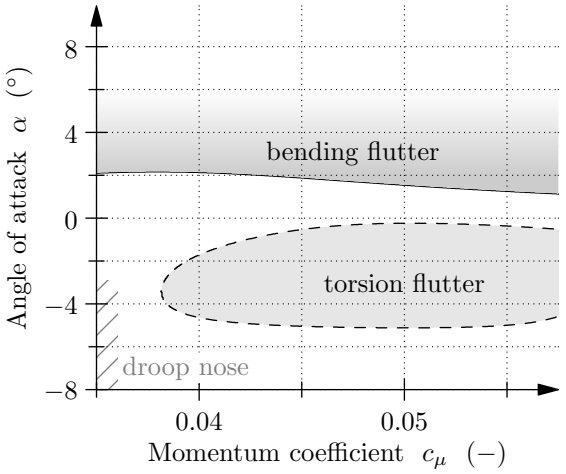

Figure 12: Stability map, clean nose

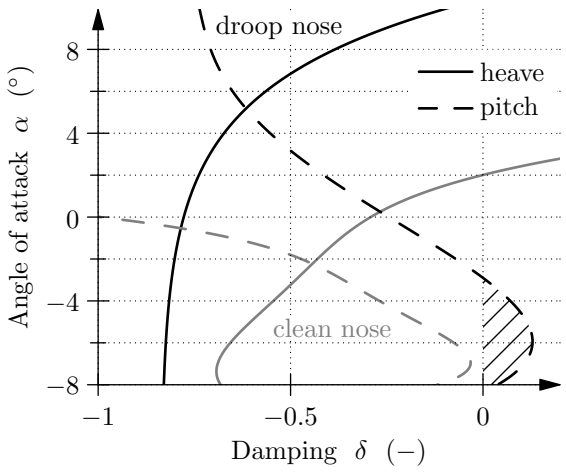

Figure 13: Damping of aerofoil motion, $c_\mu = 0.033$

The model for the droop nose is restricted to the optimal momentum coefficient of $c_\mu = 0.033$. Therefore, the same stability map cannot be given. Instead, the damping δ of the aerofoil modes

derived from the eigenvalues $\lambda = \delta \pm i\omega$ is considered for a range of angles of attack. The first mode describes heave (bending) motion, the second pitch (torsion). The damping is compared for clean and droop nose in Figure 13. The shift in bending flutter has already been mentioned above.

With a clean nose, the pitch oscillation is stable for all angles of attack, agreeing to the results given in Figure 12, while with a droop nose torsion flutter occurs in the range of $-8° \leq \alpha \leq -3°$. To match these results with the derivatives given in Figure 8, it is important to notice that for both derivatives a positive value means a destabilising effect on the pitching motion around the center of mass, while a negative value has a stabilising effect. Thus the instable area does not match the area, where $c_{M\dot{\alpha}}$ is positive, because the negative values of $c_{L\dot{\alpha}}$ prevent flutter. Still, there is a considerable range of angles, where the pitching motion is unstable, which is well inside the range of operation.

5 CONCLUSION

Investigating the aeroelastic behaviour of circulation controlled aerofoils, two additional flutter phenomena occur, which are not known from conventional aerofoils. Both of them are independent of the velocity, so that they may occur in landing approach, where the active circulation control is an essential part of the aircraft concept.

Bending flutter occurs at angles of attack beyond the maximum lift, where the lift gradually decreases with increasing angle of attack before stall. As an aircraft will usually fly well below the maximum lift for security reasons, this flight condition, though possible, will probably be less of a problem.

Torsion flutter, however, occurs at angles of attack between $0°$ and $-10°$, even if the maximum lift is shifted to $> 10°$ by the droop nose. Furthermore, it is increased by the application of a droop nose, which on the other hand is essential to make a feasible flight path possible. This aspect will have to be investigated further in order to be able to rule out the danger of torsion flutter for an aircraft with circulation controlled wings.

6 REFERENCES

[1] T. Young. Outlines of experiments and inquiries respecting sound and light. *Philosophical Transactions of the Royal Society of London*, 90:106–150, 1800.

[2] M.J. Lighthill. Notes on the deflection of jets by insertion of curved surfaces, and on the design of bends in wind tunnels. Reports and memoranda 2105, Aeronautics Research Council, 1945.

[3] G.K. Korbacher. Aerodynamics of powered high-lift systems. *Annual Review of Fluid Mechanics*, 6(1):319–358, 1974.

[4] N. Wood. Circulation control airfoils – past, present, future. Technical Report 85-0204, AIAA, 1985.

[5] K.C. Pfingsten and R. Radespiel. Experimental and numerical investigation of a circulation control airfoil. In *47th AIAA Aerospace Sciences Meeting*, Orlando, FL, 2009. AIAA 2009-533.

[6] J.B. Wilkerson. Aeroelastic characteristics of a circulation control wing. Technical Report 76-0115, David W. Taylor Naval Ship Research and Development Center, 1976.

[7] D.J. Haas and I. Chopra. Static aeroelastic characteristics of circulation control wings. *Journal of Aircraft*, 25(10):948–954, 1988.

[8] D.J. Haas and I. Chopra. Flutter of circulation control wings. *Journal of aircraft*, 26(4):373–381, 1989.

[9] R. Radespiel and W. Heinze. SFB 880: Fundamentals of high lift for future commercial aircraft. *CEAS Aeronautical Journal*, 5(3):239–251, 2014.

[10] M. Burnazzi and R. Radespiel. Design of a droopnose configuration for a Coanda active flap application. In *51th AIAA Aerospace Sciences Meeting including the New Horizons Forum and Aerospace Exposition*, Dallas (TX), 2013. AIAA 2013-0487.

[11] J. Wild. Experimental investigation of Mach- and Reynolds-number dependencies of the stall behavior of 2-element and 3-element high-lift wing sections. In *50th AIAA Aerospace Sciences Meeting*, Nashville, TN, 2012. AIAA 2012-0108.

[12] K. Sommerwerk and M.C. Haupt. Design analysis and sizing of a circulation controlled CFRP wing with Coandă flaps via CFD-CSM coupling. *CEAS Aeronautical Journal*, 5(1):95–108, 2014.

[13] D. Schwamborn, A.D. Gardner, H. von Geyr, A. Krumbein, and H. Lüdecke. Development of the DLR TAU-code for aerospace applications. In *Proceedings of the International Conference on Aerospace Science and Technology*, pages 26–28, Bangalore, India, 2008.

[14] J.H. Diekmann. Analysis of trimmable conditions for a civil aircraft with active high-lift system. *CEAS Aeronautical Journal*, 6(1):109–120, 2014.

7 ACKNOWLEDGEMENTS

Financial support has been provided by the German Research Foundation (DFG) in the framework of the Sonderforschungsbereich 880. Special thanks go to Marco Burnazzi from the Institute of Fluid Mechanics of the TU Braunschweig for creating the grids for the flow simulations.

8 COPYRIGHT STATEMENT

The authors confirm that they, and/or their company or organization, hold copyright on all of the original material included in this paper. The authors also confirm that they have obtained permission, from the copyright holder of any third party material included in this paper, to publish it as part of their paper. The authors confirm that they give permission, or have obtained permission from the copyright holder of this paper, for the publication and distribution of this paper as part of the IFASD 2015 proceedings or as individual off-prints from the proceedings.